Headgroup structure and cation binding in phosphatidylserine lipid bilayers

Hanne Antila,[1] Pavel Buslaev,[2] Fernando Favela,[3] Tiago M. Ferreira,[4] Ivan Gushchin,[2] Matti Javanainen,[5] Batuhan Kav,[1] Jesper J. Madsen,[6,7] Josef Melcr,[8] Markus S. Miettinen,[1] Ricky Nencini,[8] O. H. Samuli Ollila,[8,9,*] and Thomas J. Piggot[10]

[1]*Department of Theory and Bio-Systems, Max Planck Institute of Colloids and Interfaces, 14424 Potsdam, Germany*
[2]*Moscow Institute of Physics and Technology, Dolgoprudny, Russia*
[3]*Mexico*
[4]*NMR group - Institut for Physics, Martin-Luther University Halle-Wittenberg*
[5]*Institute of Organic Chemistry and Biochemistry of the Czech Academy of Sciences, Flemingovo nám. 542/2, CZ-16610 Prague 6, Czech Republic*
[6]*Department of Chemistry, The University of Chicago, Chicago, Illinois, United States of America*
[7]*Department of Global Health, College of Public Health, University of South Florida, Tampa, Florida, United States of America*
[8]*Institute of Organic Chemistry and Biochemistry, Academy of Sciences of the Czech Republic, Prague 6, Czech Republic*
[9]*Institute of Biotechnology, University of Helsinki*
[10]*Chemistry, University of Southampton, Highfield, Southampton SO17 1BJ, U.K*

(Dated: May 22, 2019)

Phosphatidylserine (PS) is a negatively charged lipid commonly found in eukaryotic membranes, where it interacts with proteins via nonspecific electrostatic interactions as well as specific binding; in the presence of calcium ions, PS can induce membrane fusion and phase separation. Molecular details of these phenomena remain not well understood, partly because accurate models to interpret the experimental data have not been available. Here we gather a set of experimental NMR data of C–H bond order parameters, S_{CH}, for pure PS and mixed PS:PC (phosphatidylcholine) lipid bilayers, and augment this data set by measuring with solid-state NMR S-DROSS the signs of S_{CH} in the POPS headgroup. We then use this data set to assess, in a wide range of available molecular dynamics (MD) simulation models (force fields) of PS, the accuracy of 1) the PS headgroup structures and 2) the ion binding to PS-containing membranes. We find that none of the MD models reproduce the NMR data within experimental accuracy. The best MD models, however, suggest that the carboxyl group in the PS headgroup does not rotate freely. In line with our previous results for PC lipids, none of the PS force fields correctly captures the cation binding affinity; moreover, the response of PS headgroups to bound ions can differ from experiments even *qualitatively*. The collected experimental dataset and simulation results pave the way for improvement of lipid force fields to correctly describe the biologically relevant negatively charged membranes and their interactions with ions. This work is part of the NMRlipids open collaboration project (`nmrlipids.blogspot.fi`).

INTRODUCTION

Phosphatidylserine (PS) is the most common negatively charged lipid in eukaryotic membranes. In red blood cells, for example, PS lipids compose 8.5% of the total lipid weight. The abundance, however, varies between different organelles, and up to 25-35% of the cytosolic leaflet of plasma membranes [1–3] consists of PS lipids. PS lipids are vastly important biomolecules that interact with signaling proteins [2], regulate surface charge and protein localization [4], and induce protein aggregation [5, 6]. Some protein domains interact specifically with PS lipids, while other protein sites attract PS lipids by nonspecific electrostatics and the binding can be regulated by calcium [2]. Therefore, deciphering the structural details of lipid headgroups and the details of cation binding are crucial for understanding the PS-mediated processes in the cell membranes.

Experimental studies have indicated that the PS headgroup is more rigid than the phosphatidylcholine (PC) owing to electrostatic interactions or the formation of hydrogen bonding network between the headgroups [7, 8]. While most monovalent ions interact weakly with PS-containing bilayers, multivalent cations and Li^+ are able to form strong dehydrated molecular complexes with PS lipids [9–19]. The dehydrated complexes of PS headgroups with calcium ions can even lead to phase separation [9, 10, 14–18]. Mixing PS lipids with PC lipids reduces their propensity to form strong complexes with multivalent ions and makes the PS headgroup less rigid [7, 8, 17, 18]. That said, some studies suggest Ca^{2+} has similar specific binding affinity to negatively charged and zwiterionic phospholipids, and that the increased cation binding to negatively charged lipid bilayers arises only due to the increased local cation concentration in the membrane vicinity [20, 21].

The molecular level interpretation of these observations is, however, lacking, and classical molecular dynamics (MD) simulations have been widely used in efforts to to understand the PS headgroup structure, its influence on lipid bilayer properties, and its interaction with ions [19, 22, 35, 53–63]. Unfortunately, the results have depended on the force field used. For example, recent simulations using the NBfix parameters for calcium [64] in CHARMM36 force field [22, 65], combined with 2D infrared spectroscopy, suggest that calcium ions interact only with the carboxylate group of PS lipids [62]; in contrast, the results from the same lipid model without the NBfix ion parameters, combined with NMR chemical shifts and rotational-echo double-resonance (REDOR) experiments, indicate a significant binding affinity also to the phosphate re-

TABLE I: The list of MD simulations of pure PS bilayers without additional salt along with the references to the force fields used and the MD trajectories. Notation 2×[time] indicates that two independent MD runs was conducted. Additional simulation details are given in the supplementary information. * Force field parameters for PS lipids generated for this work, for full details see the supplementary information.

lipid/counter-ions	force field for lipids	[a]N_l	[b]N_w	[c]T (K)	[d]t_{sim}(ns)	[e]t_{anal} (ns)	[f]files
POPS/Na^+	CHARMM36 [22]	128	4480	298	2×500	2×100	[23]
POPS/K^+	CHARMM36 [22]	128	4480	298	2×500	2×100	[24]
POPS/Na^+	CHARMM36-UA* [22, 25]	128	4480	298	2×500	2×100	[26]
POPS/Na^+	MacRog [27]	128	4480	298	2×500	2×100	[28]
POPS/K^+	MacRog [27]	128	4480	298	200	150	[29]
POPS/Na^+	Lipid17 [30] / JC [31]	128	4480	298	2×600	2×100	[32]
POPS/Na^+	Lipid17 [30] / ff99 [33]	128	4480	298	2×600	2×100	[34]
POPS/Na^+	Berger [35]	128	4480	298	2×500	2×100	[36]
POPS/Na^+	GROMOS-CKPM [37–39]	128	4480	298	2×500	2×100	[40]
POPS/Na^+	GROMOS-CKP [37–39]	128	4480	298	2×500	2×100	[41]
POPS/Na^+	Slipids [42]	128	4480	298	2×500	2×100	[43]
DOPS/Na^+	CHARMM36 [22]	128	4480	303	2×500	2×100	[44]
DOPS/Na^+	CHARMM36-UA* [22, 25]	128	4480	303	2×500	2×100	[45]
DOPS/Na^+	Lipid17 [30] / JC [31]	128	4480	303	2×600	2×100	[46]
DOPS/Na^+	Lipid17 [30] / ff99 [33]	128	4480	303	2×600	2×100	[47]
DOPS/Na^+	Berger [35]	128	4480	303	2×500	2×100	[48]
DOPS/Na^+	GROMOS-CKPM* [39]	128	4480	303	2×500	2×100	[49]
DOPS/Na^+	GROMOS-CKP* [39]	128	4480	303	2×500	2×100	[50]
DOPS/Na^+	Slipids [42]	128	4480	303	2×500	2×100	[51]
DOPS/Na^+	Slipids [42]	288	11232	303	200	100	[52]

[a]Number of lipid molecules with largest mole fraction
[b]Number of water molecules
[c]Simulation temperature
[d]Total simulation time
[e]Time used for analysis
[f]Reference for simulation files

gion [63]. Meanwhile, simulations with the Berger force field [35, 66], combined with fluorescent and vibrational sum frequency spectroscopy, suggest substantial calcium binding also to the carbonyls in the acyl chains [61].

We have recently demonstrated that the lipid C–H bond order parameters, S_{CH}, can be utilized to resolve such controversies [67, 68]. The S_{CH} can be measured from NMR experiments with high accuracy and directly compared to simulations in order to evaluate the simulation model quality or to interpret the experiments [69]. Using this approach, it has been established that the structure of PC lipid headgroup and glycerol backbone are not well captured by most MD force fields [67], that the cation binding to PC lipid bilayers is overestimated [68], and that the splitting of the order parameters at carbon 2 in *sn*-2 lipid tails is correctly reproduced only in the CHARMM36 force field [70].

Here, we extend the available set of experimentally measured PS lipid headgroup and glycerol backbone C–H bond order parameters by measuring the signs of the order parameters using S-DROSS solid-state NMR spectroscopy. The quality of headgroup structures and the ion binding affinity in the available MD simulation models of PS lipids are then asessed based on the collected experimental data. The results pave the way for development of lipid models that correctly describe the headgroup region of negatively charged lipids in physiological salt conditions. Such force fields are expected to be useful in understanding biological function of lipid headgroups and glycerol backbone, as these are known to behave similarly in simple model membranes and in cells [20, 71, 72].

METHODS

Experimental C–H bond order parameters

The headgroup and glycerol backbone C–H bond order parameter magnitudes of 1-palmitoyl-2-oleoyl-*sn*-glycero-3-phospho-L-serine (POPS) were determined by measuring the chemical-shift resolved dipolar splittings with a R-type Proton Detected Local Field (R-PDLF) experiment [94]. The corresponding order parameter signs were measured with a S-DROSS experiment [95] using natural abundance ^{13}C solid state NMR spectroscopy as described previously [96, 97]. The

TABLE II: The list of POPC:POPS mixtures simulated with different molar fractions and different amounts of added calcium. The salt concentrations are calculated as [salt]=$N_c \times$[water] / N_w, where [water] = 55.5 M. This corresponds the concentration in buffer before solvating lipids, which are reported in the experiments by Roux et al. [17]. Notation 2×[time] indicates that two independent MD runs was conducted. The simulation details are given in the supplementary information. * Force field parameters for PS lipids generated for this work, for full details see the supplementary information.

lipid/counter-ions	force field for lipids / ions	[$CaCl_2$] (M)	[a]N_l	[b]N_w	[c]N_c	[d]T (K)	[e]t_{sim}(ns)	[f]t_{anal} (ns)	[g]files
POPC:POPS (5:1)/K^+	CHARMM36 [22, 65]	0	250	11207	0	298	200	180	[73]
POPC:POPS (5:1)/K^+	CHARMM36 [22, 65]	0	110	4620	0	298	2×500	2×100	[74]
POPC:POPS (5:1)/Na^+	CHARMM36 [22, 65]	0	110	4620	0	298	2×500	2×100	[75]
POPC:POPS (5:1)	CHARMM36 [22, 64, 65]	0.26	250	11190	53	298	200	180	[76]
POPC:POPS (5:1)	CHARMM36 [22, 64, 65]	1.06	250	11174	214	298	200	180	[77]
POPC:POPS (1:1)/K^+	CHARMM36 [22, 65]	0	150	10785	0	298	200	180	[78]
POPC:POPS (1:0)	MacRog [27]	0	120	5120	0	298	200	150	[79]
POPC:POPS (5:1)/K^+	MacRog [27]	0	120	5760	0	298	400	250	[80]
POPC:POPS (5:1)/K^+	MacRog [27]	0.10	120	5760	10	298	600	300	[80]
POPC:POPS (5:1)/K^+	MacRog [27]	0.30	120	5760	31	298	600	300	[80]
POPC:POPS (5:1)/K^+	MacRog [27]	1.00	120	5760	104	298	600	300	[80]
POPC:POPS (5:1)/K^+	MacRog [27]	3.00	120	5760	311	298	600	300	[80]
POPC:POPS (5:1)/K^+	Lipid14/17 [30, 81]	0	120	5760	0	298	2×500	2×200	[82]
POPC:POPS (5:1)/Na^+	Lipid14/17 [30, 81]	0	120	5760	0	298	2×500	2×200	[83]
POPC:POPS (5:1)	Lipid14/17 [30, 81]	0.50	120	5760	52	298	2×500	2×200	[84]
POPC:POPS (5:1)	Lipid14/17 [30, 81]	1.00	120	5760	104	298	2×500	2×200	[84]
POPC:POPS (5:1)	Lipid14/17 [30, 81]	2.00	120	5760	208	298	2×500	2×200	[84]
POPC:POPS (5:1)	Lipid14/17 [30, 81]	3.00	120	5760	311	298	2×500	2×200	[84]
POPC:POPS (5:1)	Lipid14/17 [30, 81]	4.00	120	5760	415	298	2×500	2×200	[84]
POPC:POPS (5:1)/Na^+	Lipid14/17 [30, 81]	0	60	3600	0	298	1000	1000	[85]
POPC:POPS (5:1)/Na^+	Lipid14/17 [30, 81, 86, 87]	0.08	60	3561	5	298	1000	1000	[85]
POPC:POPS (5:1)/Na^+	Lipid14/17 [30, 81, 86, 87]	0.13	60	3561	8	298	1000	1000	[85]
POPC:POPS (5:1)/Na^+	Lipid14/17 [30, 81, 86, 87]	0.20	60	3561	13	298	1000	1000	[85]
POPC:POPS (5:1)/Na^+	Lipid14/17 [30, 81, 86, 87]	0.41	60	3522	26	298	1000	1000	[85]
POPC:POPS (5:1)/Na^+	Lipid14/17 [30, 81, 86, 87]	0.62	60	3483	39	298	1000	1000	[85]
POPC:POPS (4:1)/Na^+	Berger [35, 88]	0	102	4290	0	310	120	80	[89]
POPC:POPS (4:1)	Berger [35, 88]	0.102[h]	104	4306	24	310	300	100	[90]
POPC:POPS (4:1)	Berger [35, 88]	0.715[h]	104	4306	72	310	300	100	[91]
POPC:POPS (5:1)/Na^+	GROMOS-CKP* [39]	0	110	4620	0	298	2×500	2×100	[92]
POPC:POPS (5:1)/Na^+	GROMOS-CKPM* [39]	0	110	4620	0	298	2×500	2×100	[93]

[a]Number of POPC molecules
[b]Number of water molecules
[c]Number of additional cations
[d]Simulation temperature
[e]Total simulation time
[f]Time used for analysis
[g]Reference for simulation files
[h]Calculation of concetration complicated by the usage scaled ions. Concentration taken as reported in the delivered data.

experiments were done in a Bruker Avance III 400 spectrometer operating at a ^{1}H Larmor frequency of 400.03 MHz. Magic angle spinning (MAS) of the sample was used at a frequency of 5.15 kHz (R-PDLF experiment) and 5 kHz (S-DROSS experiment). The following experimental setups were used.

C–H bond order parameters from the R-PDLF experiment. The parameters are described according to Figures 1c and 2c of the original reference for the R-PDLF experiment [94]. The refocused-INEPT delays were $\tau_1 = 1.94$ ms and $\tau_2 = 0.97$ ms. The used radio frequency pulses had the following nutation frequencies: 46.35 kHz ($R18_1^7$ pulses), 63.45 kHz (^{13}C 90^o

and 180°), 50 kHz (SPINAL64 ^{1}H decoupling pulses). The t_1 increment was equal to 10.79 μs $\times 18 \times 2$, and 32 points in the indirect dimension were recorded using 1024 scans for each, with a recycle delay of 5 s and a spectral width of 149.5 ppm.

Order parameter signs from the S-DROSS experiment. The parameters are described according to Figures 1b and 1c of the original reference for the S-DROSS experiment [95]. The refocused-INEPT delay δ_2 was 1.19 ms. The τ_1 and τ_2 in the S-DROSS recoupling blocks R were set as $\tau_1 = 39.4\,\mu$s and $\tau_2 = 89.4\ \mu$s. The used radio frequency pulses had the nutation frequencies: 63.45 kHz (^{13}C 90° and 180°), 50 kHz (^{1}H SPINAL64 decoupling). The t_1 increment (dipolar recoupling dimension) was 800 μs, and a total of 8 points along t_1 were measured using 1024 scans for each, with a recycle delay of 5 s and a spectral width of 149.5 ppm.

Numerical simulations of S-DROSS curves. The numerical simulations of S-DROSS curves were performed using the SIMPSON simulation package [98] by inputing the ^{13}C–^{1}H dipolar couplings, either as determined by the R-PDLF experiments, or as calculated from the known ^{2}H quadrupolar couplings [7]. The chemical shift anisotropy and homonuclear couplings were neglected, and the SIMPSON input file *rep2000* was used to simulate a random distribution of bilayer orientations in the samples studied.

Sample preparation. The sample was prepared simply by mixing POPS powder (1-palmitoyl-2-oleoyl-*sn*-glycero-3-phospho-L-serine, purchased from Avanti Polar Lipids as sodium salt) with water (lipid:water 60:40 wt-%) in an Eppendorf tube by mixing and centrifuging the sample approximately 5 to 6 times until a homogeneous viscous fluid was visually observed. Then 20 mg of the sample was transferred to an NMR insert suitable for 4 mm NMR rotors.

Molecular dynamics simulations

Molecular dynamics simulation data were collected using the Open Collaboration method [67], with the NMRlipids Project blog (`nmrlipids.blogspot.fi`) and GitHub repository (`github.com/NMRlipids/NMRlipidsIVotherHGs`) as the communication platforms. The simulated systems are listed in Tables I (pure PS bilayers without additional ions) and II (mixed PC:PS bilayers at various salt concentrations). Further simulation details are given in the SI, and the simulation data are indexed in a searchable database available at `www.nmrlipids.fi`, and in the NMRlipids/MATCH repository (`github.com/NMRlipids/MATCH`).

The C–H bond order parameters were calculated directly from the carbon and hydrogen positions using the definition

$$S_{\mathrm{CH}} = \frac{1}{2}\langle 3\cos^2\theta - 1\rangle, \qquad (1)$$

where θ is the angle between the C–H bond and the membrane normal (taken to align with z, with bilayer periodicity in the xy-plane). Angular brackets denote average over all sampled configurations. The order parameters were calculated by first averaging over time separately for each lipid in the system, and then calculating the average and the standard error of the mean over the different lipids. The analysis can be conducted using a Python program (`calcOrderParameters.py`, available in Ref. 99) that utilizes the MDAnalysis library [100, 101]. For united atom models, the positions of hydrogens were generated before the order parameter calculation using `protonate` tool of the Gromacs 3 sofware package [102]. The ion number density profiles were calculated using the `gmx density` tool of the Gromacs sofware package [102].

Comparison of ion binding to negatively charged lipid bilayers between simulations and experiments using the molecular electrometer concept

The order parameters of the α and β carbons in the PC headgroup decrease proportionally to the amount of positive charge bound to the bilayer [103–105], and can therefore be used to measure the ion binding affinity. This concept, known as the molecular electrometer, is especially useful for comparison between simulations and experiments, as the headgroup order parameters at varying cation concentrations can be easily calculated from simulations [68]. The headgroup order parameters of negatively charged PS and PG lipids also exhibit systematic, but less understood dependencies on the bound charge [17, 106–108]. Therefore, measuring the PC headgroup order parameters from mixed (here PS:PC) bilayers [17, 18, 108] (see also SI section S2) provides a more straightforward way of characterizing the ion binding to negatively charged membranes.

Calibrating the PC order parameter response to a known amount of bound charge [68, 109] is an important preliminary step for using the molecular electrometer concept. This can be done using experimental data from mixtures of monovalent cationic surfactants (dihexadecyldimethylammonium) and POPC [109, 110], (see SI section S3). Additionally, we quantify the response of PC headgroup order parameters to the negatively charged PS, which also follows the molecular electrometer concept in experiments [72] (see SI section S2).

Studies applying the molecular electrometer concept have utilized two different definitions for salt concentration: the concentrations are reported either in water before solvating the lipids [17, 68, 103], or in bulk water after solvating the lipids [104, 109]. In this work, we use the former definition to be consistent with the reference experimental data [17]. However, the choice of definition has only a marginal effect to the results in simulations with realistic ion binding affinity (see SI section S4).

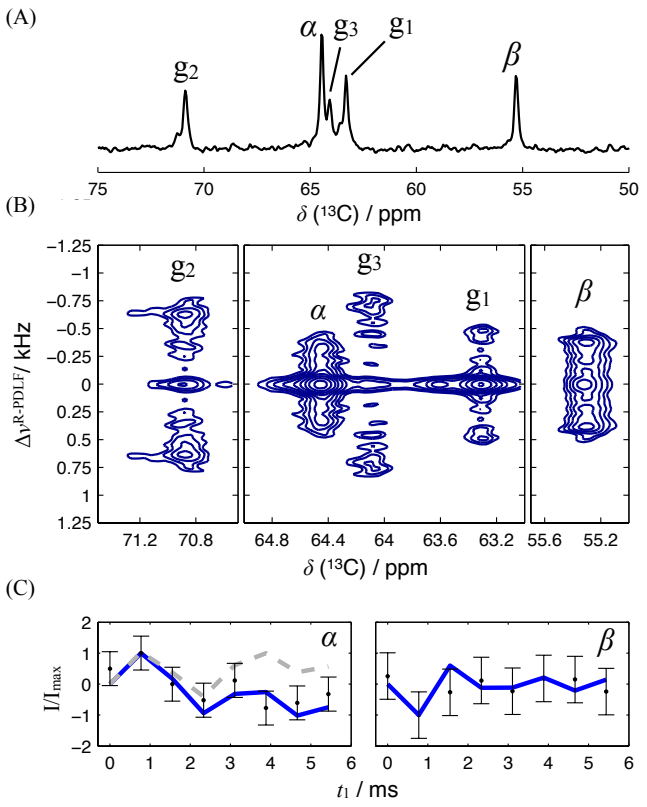

FIG. 1: The headgroup and glycerol backbone region of the (A) INEPT spectrum and (B) 2D R-PDLF spectra. (C) Experimental S-DROSS data (points), and SIMPSON simulations (blue lines) with the C–H bond order parameter values of -0.12 for the β-carbon, and +0.09 and -0.02 for the α-carbon. Dashed gray line is the S-DROSS curve from a SIMPSON simulation with a positive value (+0.02) for the smaller α-carbon C–H bond order parameter.

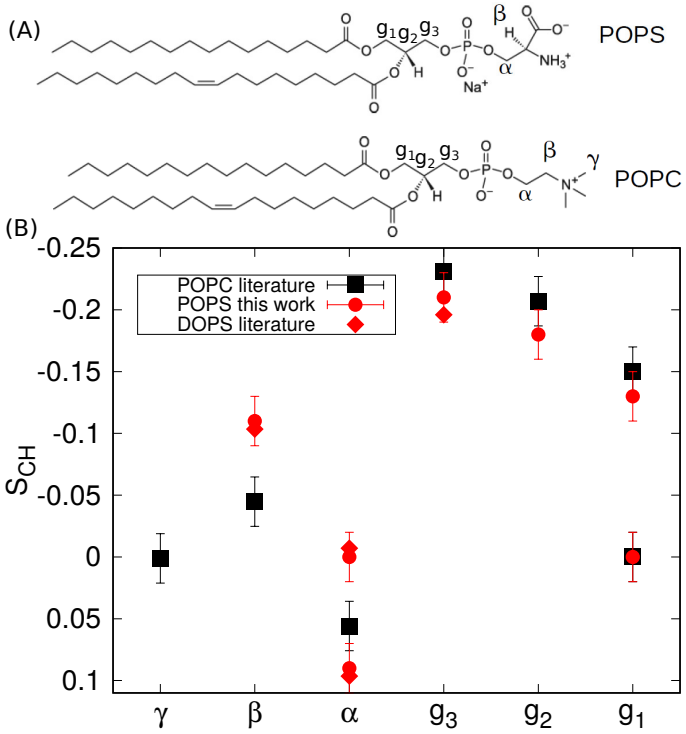

FIG. 2: (A) Chemical structures and labels for the headgroup and glycerol backbone carbons. (B) Headgroup and glycerol backbone order parameters of POPS (T = 298 K) measured in this work compared with the previously published values from DOPS (T = 303 K, ^{2}H NMR, 0.1M of NaCl) [7] and POPC (T = 300 K, ^{13}C NMR) [96] experiments. Signs of the PS order parameters are measured in this work whereas signs of the PC order parameters are measured previously [97]. The size of errorbars ($\pm$0.02) shown for ^{13}C NMR data is justified previously [67, 69].

1.Replacing the "literature" with "from Ref X" has been suggested https://github.com/NMRLipids/NMRlipidsIVotherHGs/issues/34. We can do this just before submission when citation numbers will not change anymore.

RESULTS AND DISCUSSION

Headgroup and glycerol backbone order parameters of POPS from ^{13}C NMR

The INEPT and 2D R-PDLF experiments from POPS sample give well resolved spectra for all the carbons in the headgroup and glycerol backbone regions (Fig. 1). The glycerol backbone carbon peaks were assigned according to the POPC spectra [96] whereas the peaks for β and α carbons were assigned according to the known order parameters from the ^{2}H NMR experiments [7]. Slices of the R-PDLF spectra and the resulting order parameter values are shown in the supplementary information (Fig. S6).

Since the R-PDLF and previous ^{2}H NMR experiments [7, 18] give only the absolute values of order parameters, we determined the signs of the PS headgroup order parameters using the S-DROSS experiment [95]. For a given carbon, its S-DROSS dipolar modulation profile in the indirect dimension is a superposition of sinusoidal functions from the possible orientations of crystallites in the sample (or bilayer patches). We phase corrected the 2D spectrum in the direct dimension such that positive and negative signs for the C—H bond order parameter give rise to profiles that initially increase and decrease, respectively. In practice, we use the known negative sign of the acyl chain carbons as a reference to perform the phase correction and interpret the distinct initial slopes of the S-DROSS profiles (Fig. S6). The S-DROSS slice for the β-carbon clearly shows an initial decrease and therefore its order parameter must be negative. For the α-carbon such analysis is not as trivial due to the two inequivalent order parameters of the two distinct C—H bonds. However, the beginning of its S-DROSS slice suggests that the larger order parameter of the alpha-carbon is positive and the decrease towards negative values at longer t_1 suggests that the smaller order parameter is negative. This is confirmed by a SIMPSON simulation using the order parameter values of +0.09 from dipolar coupling measured here (Fig. S6) and -0.02 from the ^{2}H NMR experiment [18]. The literature value for the smaller order parameter was used because the resolution of our R-PDLF experiment

was not sufficient to determine the small value of the order parameter. The S-DROSS curve from SIMPSON simulation with a positive value for the smaller order parameter (dashed grey in Fig. 1 C)) did not agree with the experiment, corroborating the interpretation that the smaller order parameter is negative.

The headgroup and glycerol backbone order parameters of POPS measured in this work are in good agreement with the previously reported values from ^{2}H NMR experiments of DOPS [7] (Fig. 2). When compared with the previously measured values for POPC [96] (Fig. 2), the β-carbon order parameter is significantly more negative and α-carbon experiences substantial forking (different order parameters for the two hydrogens in the same carbon [69]) in the PS headgroup. These features have been intepreted to arise from a rigid PS headgroup conformation, stabilized by hydrogen bonds or electrostatic interactions [7, 8], but detailed structrural interpretation is not available.

We note that the the DOPS ^{2}H NMR reference data found in the literature [7, 17] was obtained by first solvating the lipids with a buffer solution and then centrifuging the sample to a pellet that was used for the measurements. Such samples have a lower lipid concentration (approximately 10 wt % of lipids [7, 17, 111]) than gravimetric samples (60 wt %) and simulations (approximately 50-60 wt %) in this work. Larger multilamellar repeat distances are expected in the samples with lower lipid concentrations due to the swelling caused by electrostatic repulsion in pure PS lipid systems [112]. Yet the PS headgroup order parameters measured from gravimetric samples (POPS) in this work are in good agreement with the results from centrifuged samples [7]. This, together with the rapid decrease of equilibrium repeat distance with addition of monovalent salt [112, 113], indicates that the hydration levels of multilamellae are sufficiently similar in the simulations and reference experiments.

Headgroup and glycerol backbone in simulations of PS lipid bilayers without additional ions

The different PS MD models produce highly varied headgroup and glycerol backbone order parameters (Fig. 3) and structures (Fig. S9 and section S6 in the SI), as previously observed also for PC lipids [67], and none of the models produces a set of order parameters in full agreement with the experiments. The models perform generally less well for PS than for PC (Figs. 3 and 5 vs. Figs. 2 and 4 in Ref. [67]). which complicates the interpretation of structural differences between PC and PS headgroups. However, concentrating on the headgroup, we see that the best performing models (Slipids, CHARMM36 and CHARMM36-UA) do replicate the larger-than-in-PC forking of the α-carbon observed in the experiments and that the Slipids force field additionally correctly produces the significantly smaller β-carbon order parameter for PS compared to PC (Fig. 3 vs. Fig. 2 in Ref. 67) also observed in the experiments (Fig. 2).

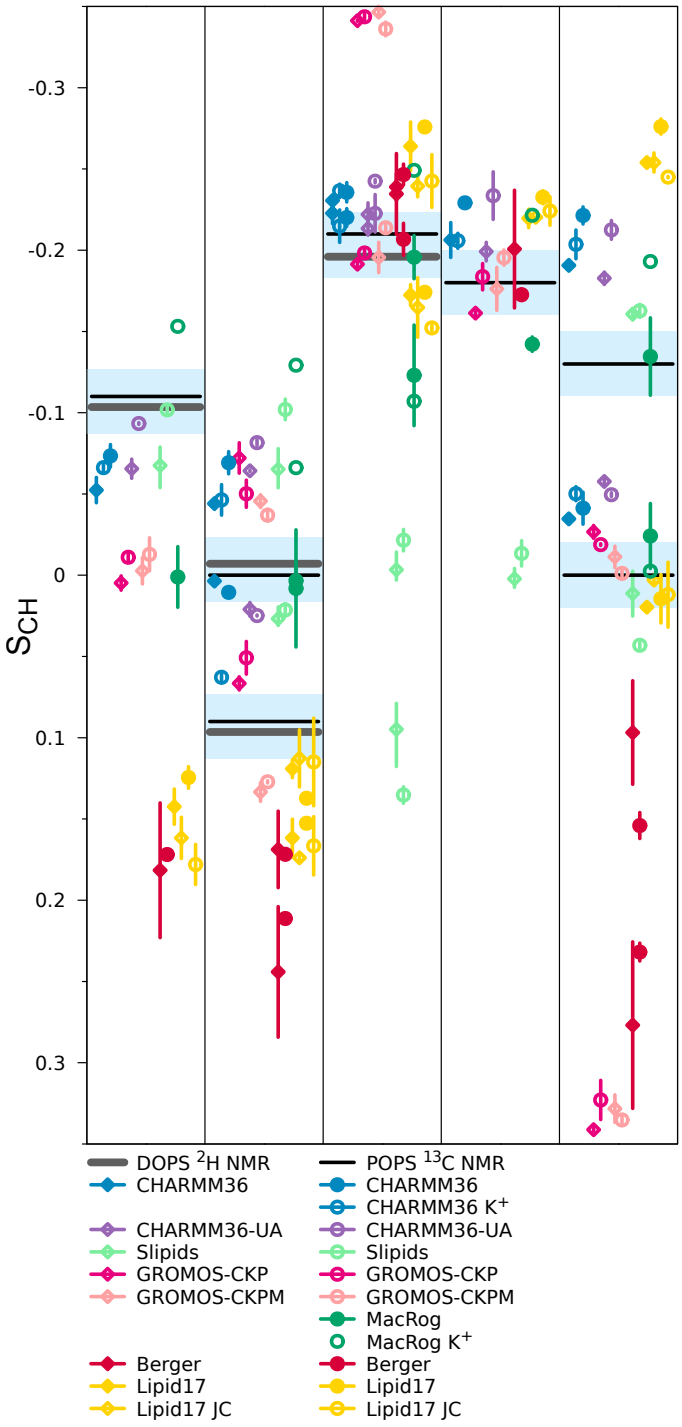

FIG. 3: Order parameters of PS headgroup (β and α) and glycerol backbone (g_3, g_2, g_1) from NMR experiments (horizontal lines), and MD simulations with different force fields (symbols). Experimental data for DOPS are measured with 0.1 M of NaCl [7], while all the other data are without additional salt. The data for DOPS is at 303 K and the data for POPS is at 298 K. Light blue areas span 0.04 units around the average of the extremal experimental values, in accordance with the expected quantitative accuracy of experiments [69]. The vertical bars shown for all simulation values (excl. MacRog K$^+$) are not error bars, but demonstrate that for these systems we had at least two data sets; the ends of the bars mark the extreme values from the sets, and the symbol marks their measurement-time-weighted average.

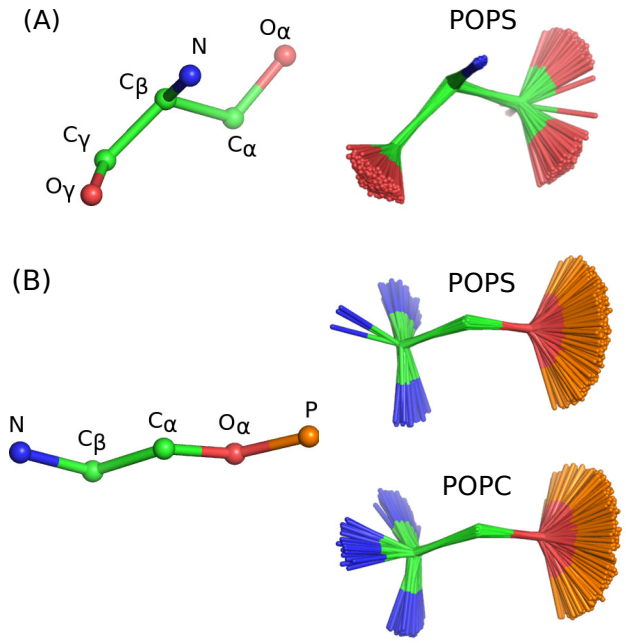

FIG. 4: Overlayed snapshots from simulations conducted with CHARMM36—the force field producing the best agreement with experiments—demonstrate the conformational fluctuations around (A) C_α-C_β-C_γ-O_γ and O_α-C_α-C_β-N of PS headgroup and (B) N-C_β-C_α-O_α and C_β-C_α-O_α-P dihedrals of PS and PC headgroups. The trajectory used for CHARMM36 POPC is available at 114.

	β	α	g_3	g_2	g_1	Σ
CHARMM 36 K+	M	M	M F	M	**M** F	7
CHARMM 36	M	**M** F	M	M	**M** F	8
CHARMM 36-UA	M	**M**	M	M	**M** F	9
MacRog K+	M	**M** F	**M F**	M	M **F**	11
MacRog	**M**	**M F**	**M F**	M	M	14
GROMOS-CKP	**M**	M F	**M F**		**M F**	14
GROMOS-CKPM	**M**	M **F**	**M F**		**M F**	14
Berger	**M**	**M F**	M F		**M** F	14
Slipid	M	**M**	**M F**	**M**	M **F**	14
Lipid17	**M**	**M F**	**M F**	M	**M F**	18
Lipid17 JC	**M**	**M** F	M **F**	M	**M F**	18

FIG. 5: Rough subjective ranking of force fields based on Figure 3. Here M indicates a magnitude problem, F a forking problem; letter size increases with problem severity. Color scheme: "within experimental error" (dark green), "almost within experimental error" (light green), "clear deviation from experiments" (light red), and "major deviation from experiments" (dark red). The Σ-column shows the total deviation of the force field, when individual carbons are given weights of 0 (matches experiment), 1, 2, and 4 (major deviation). For full details of the assessment, see Supplementary Information.

Interestingly, the three models that best fit the experimental data have a narrower distribution in the C_α-C_β-C_γ-O_γ dihedral angle (single peak around 120°) in comparison to the other models which yield a distribution between two angles (Fig. S7). The restricted motion is also visible in the sampled conformations (Figs. 4 (A) and S9) suggesting that the rotation of the carboxyl group is limited in the serine headgroup. In addition, the N-C_β-C_α-O_α dihedral exhibits a more asymmetric angle distribution for PS than for PC headgroup in CHARMM36 and Slipids simulations that have the best agreement with experiments (Figs. 4 (B) and S10).

These results might reflect the increased rigidity proposed in the early experimental studies [7, 8], and the suggested characteristic conformations of the PS headgroup can be useful when interpreting experiments. However, as the none of the tested models fully reproduces the experimental order parameters, more accurate MD force fields are required to confirm the correct conformational ensemble.

Counterion binding and interactions between PC and PS headgroups

Membranes containing PS lipids are always accompanied with counterions that modulate electrostatic interactions between lipids and other biomolecules. MD simulations have suggested that counterions reduce the area per lipid of PS bilayers compared to PC bilayers [35, 54, 55] by screening the repulsion between charged lipid headgroups. We explore this by quantifying the counterion density profiles along the membrane normal accompanied by the areas per lipid in Fig. 6. The force fields studied show significant differences in both binding affinity and distribution of ions at the interface. The experimental area per lipid (62.7 ± 1.3 Å^2) [59] is reproduced only in GROMOS-CKP and in the MacRog simulation with potassium counterions, while other models give considerably smaller values (Fig. 6). However, the counterion binding and the concomitant electrostatic screening of the headgroup repulsion does not fully explain the low area per molecule val-

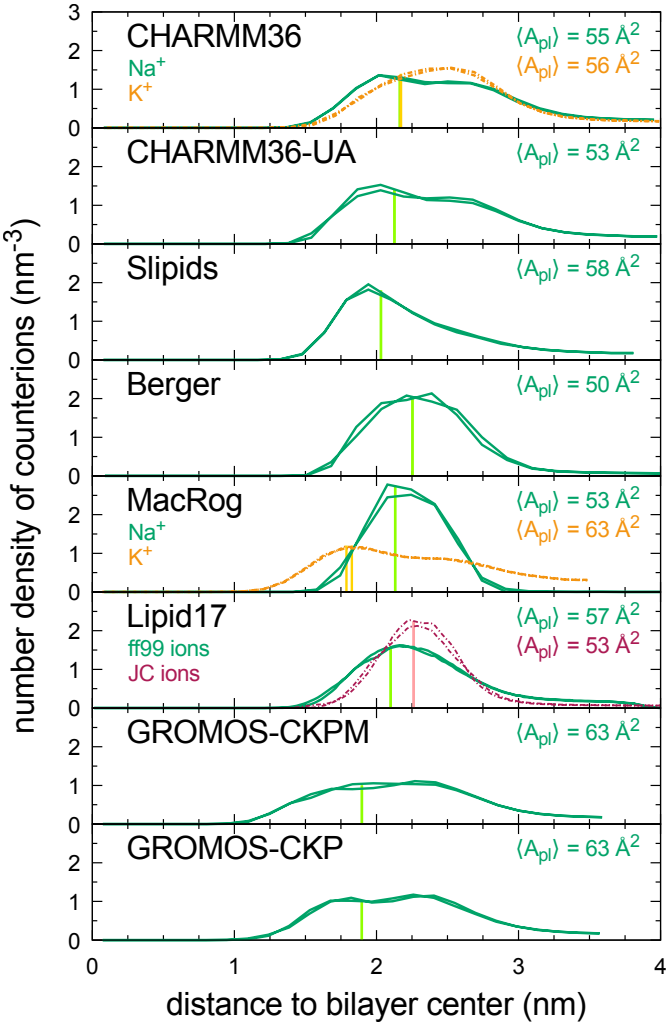

FIG. 6: Counterion density profiles along the membrane normal and areas per lipid (A_{pl}) of POPS lipid bilayer from simulations with different force fields. The vertical green bars indicate the location of the phosphate density peak. The experimental area per lipid is 62.7 ± 1.3 Å^2 [59].

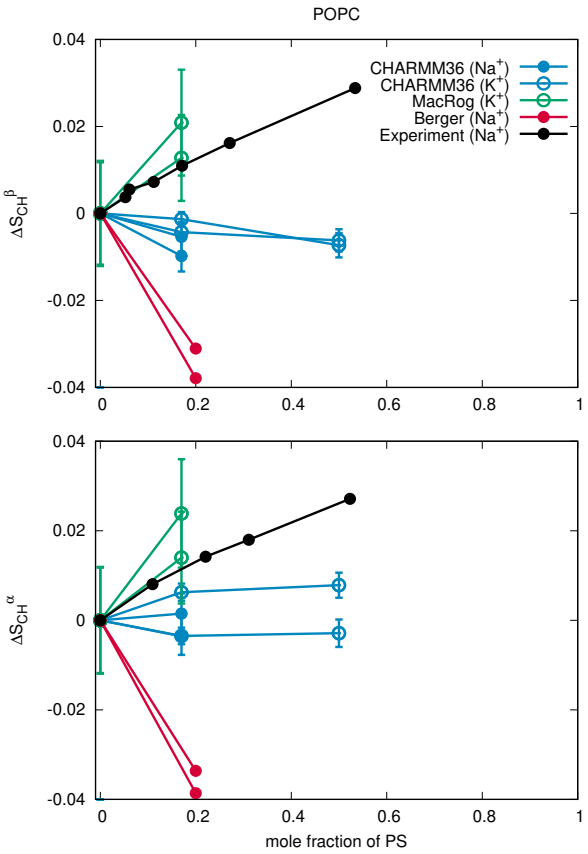

FIG. 7: Changes of POPC headgroup order parameters with increasing amount of POPS in POPC:POPS mixtures at 298 K. Experimental values are from Ref. 72 with the signs measured in Ref. 97. The value from the CHARMM36 simulation with sodium is the average of two independent simulations and the error bar is given as the difference between the results divided by two.

2.After we know which force field is used for POPC in GROMOS-CKP simulations, we might be able to add GROMOS-CKP data into this plot.

ues since the MacRog simulation, which has the strongest sodium binding (the lowest concentrations in bulk water), gives the same area per molecule as the CHARMM36-UA simulation, which has significantly weaker counterion binding affinity. On the other hand, MacRog simulations with potassium produce a larger area per molecule (63 Å^2) than with sodium (53 Å^2) in line with the weaker potassium binding affinity (Fig. 6). The results are in line with the previous study suggesting that the low areas per molecule in PS lipid bilayers originate from the combination of both the counterion binding and intermolecular interactions between lipid headgroups [115].

The experimentally observed modulation of headgroup order parameters by increasing salt concentration (the molecular electrometer concept) has been previously used to evaluate the cation binding to zwitterionic PC bilayers in simulations [68]. Studying binding of cations to negatively charged lipid bilayers is less straighforward due to the presence of cationic counterions (the lack of a ion-free reference state) and the analysis is further complicated by the artificial aggregation of counterions observed in some simulations (section S7 in the SI) Therefore, we evaluate here the amount of bound charge not by adding salt (although this is discussed in the SI section S7), but by studying the changes of the headgroup order parameters with increasing amount of negatively charged lipids (and thus increasing amount of cationic counterions) in the bilayer.

Experimentally, the headgroup order parameters of POPC increase when negatively charged POPS lipids are incorporated in lipid bilayer (section S1) [72, 105]. This is reproduced in the MacRog simulations with potassium counterions (Fig. 7), which have the weakest binding affinity to POPS lipid bilayers (Fig. 6). The CHARMM36 and Berger simulations either exhibit no change or show a decrease in the

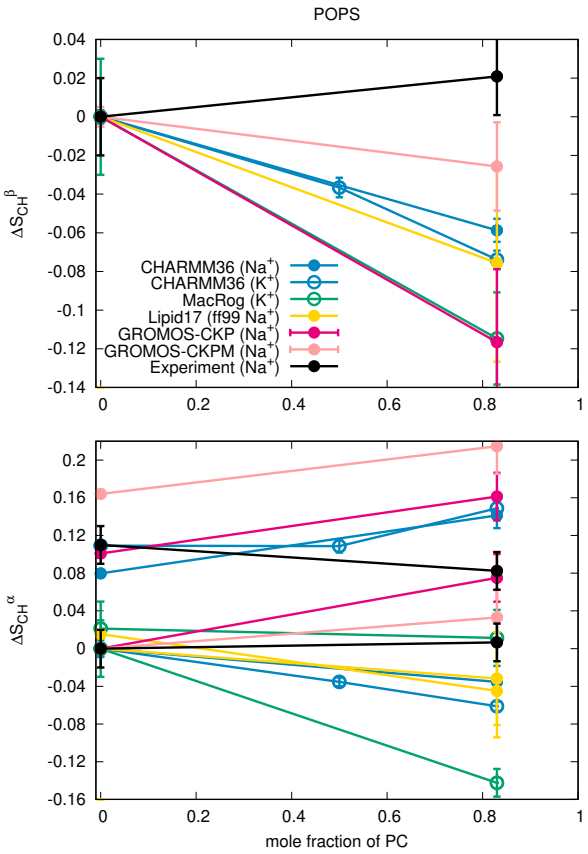

FIG. 8: Modulation of POPS headgroup order parameters with increasing amount of POPC in POPC:POPS mixtures at 298 K. Experimental values with the signs are measured for pure POPS system in this work. The signs are assumed to be the same for the mixture and the values are from Ref. 17. Because the experimental values of POPS in pure and mixed bilayers come from ^{13}C NMR (this work) and ^{2}H NMR (Ref. 17), respectively, the error bars of 0.02 are used here [67, 69]. The y-axis for the α-carbon results of POPS (bottom) is shifted with the same value for both order parameters such that the lower order parameter value from pure POPS is at zero to correctly illustrate the significant forking. The values from CHARMM36 and GROMOS simulations are averages of two independent simulations and the error bars are given as the difference between the results divided by two.

POPC headgroup order parameters as the amount of POPS increases (Fig. 7). Therein, the stronger counterion binding cancels the effect of negatively charged headgroups and prevents the experimentally observed increase of headgroup order parameters with growing amount of PS lipids. Therefore, we suggest that the relatively weak binding of potassium in the MacRog simulations (Fig. 6) produces the most realistic surface charge density in membranes containing PS lipids, while the other tested models overestimate the counterion binding affinity. The results are in line with the behaviour of headgroup order parameters as a function of added counterions analyzed in section S7 in the SI.

The reduced forking of the POPS α-carbon (Fig. 8) together with other experimental results suggest that the PS headgroup structure becomes less rigid when diluted with POPC [7, 8, 17, 18, 72]. Unfortunately, none of the tested models correctly reproduce the modulation of POPS headgroup order parameters with increasing amount of POPC in POPC:POPS mixtures (Fig. 8) and more accurate force fields are needed to correctly describe the PC-PS headgroup interactions in MD simulations.

Ca^{2+} binding affinity to bilayers with negatively charged PS lipids

Calcium binding affinity to membranes containing the negatively charged PS lipids can be experimentally quantified by measuring the PC lipid headgroup order parameters from POPC:POPS (5:1) mixtures (section S2), where the measurement is not compromised by the dehydrated lipid-ion complexes and phase separation, and the bilayer remains uniform [15–18]. Despite the lack of an ion-free reference state in the presence of negatively charged lipids, our simulations give coherent results for POPC headgroup order parameters as a function of $CaCl_2$ in the POPC:POPS (5:1) mixtures (Fig. 9). As expected from the previous study of pure PC lipid bilayers [68], almost all the tested simulation models overestimate the experimentally observed [17] decrease of the POPC headgroup order parameters upon increasing Ca^{2+} concentration (Fig. 9), indicating too strong calcium binding affinity. The only exception is the CHARMM36 simulation utilizing the NBfix interaction for calcium [64], wherein the modulation of order parameters is underestimated, indicating weaker binding affinity than in experiments. Notably, CHARMM36 simulations with the NBfix corrections [22, 64] give similar binding affinities of calcium and sodium to POPC bilayer (see section S8), in contrast to the experiments [103, 104, 117]. This suggests that the calcium binding affinity is underestimated in CHARMM36 simulations when using the NBfix for calcium [64], but overestimated in all the other tested models. This is evident in the calcium density distributions where almost all Ca^{2+} ions bind to the membrane interface in all simulation models except CHARMM36 (Fig. 10).

Experimentally, the POPS headgroup order parameters in POPC:POPS (5:1) mixtures exhibit a strong dependence of $CaCl_2$ with small concentrations that saturates below 100 mM (Fig. 9). The β-carbon order parameter increases with added $CaCl_2$, whereas the larger α-carbon order parameter decreases; a slight increase is observed in the smaller α-carbon value. All these changes are significantly overestimated in the tested simulation models, including CHARMM36 which underestimated the binding affinity. Importantly, the different simulation models predict qualitatively different behaviour for the two POPS α-carbon order parameters with added calcium. For example, both order parameters decrease in Berger, but increase in MacRog, and in Lipid14/17 and CHARMM36 a more complicated behavior is seen. This is in contrast to the PC headgroup, where qualitatively correct reponse to bound

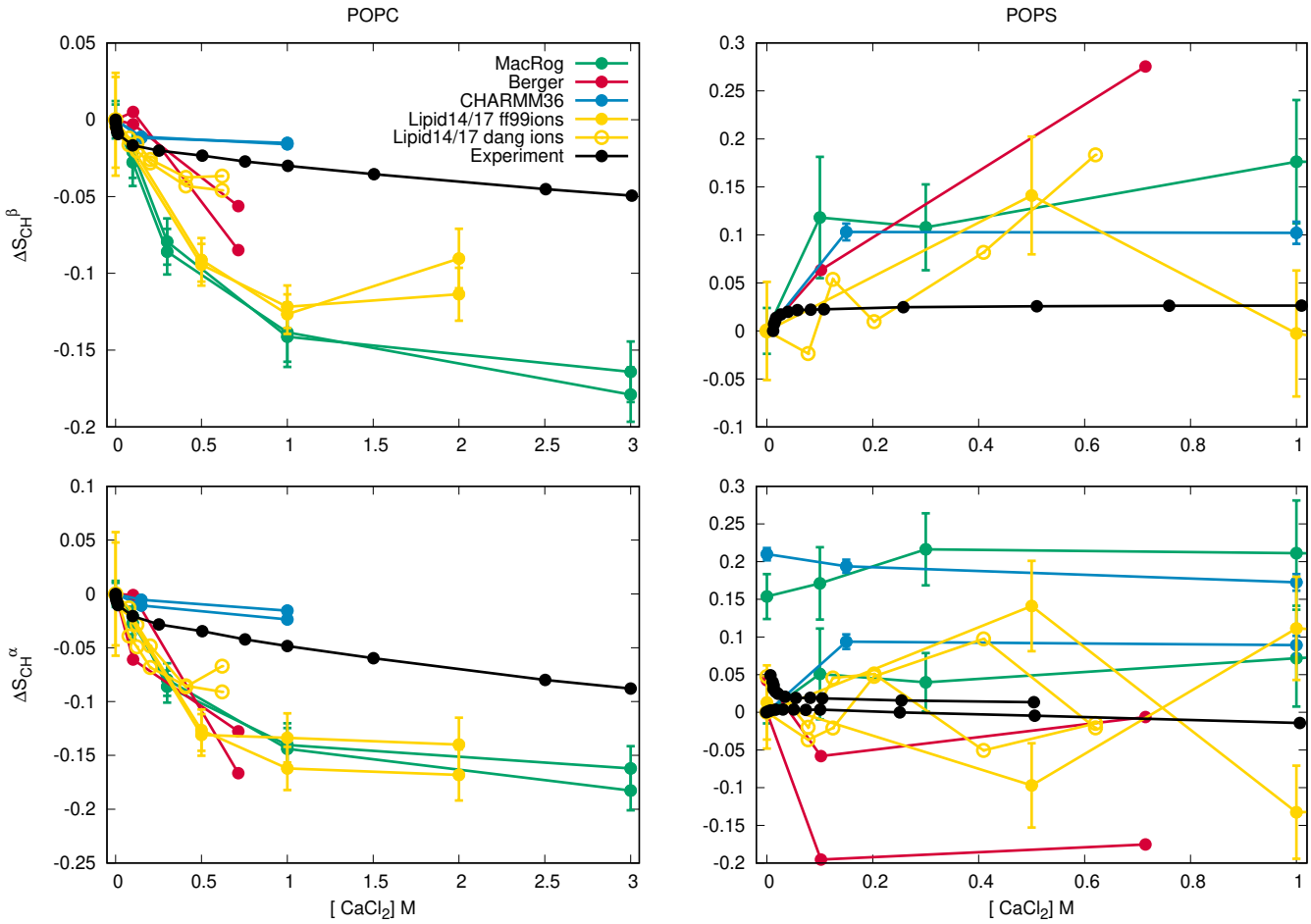

FIG. 9: Variation of POPC (left) and POPS (right) headgroup order parameters from POPC:POPS (5:1) mixture as a function $CaCl_2$ concentration from experiments [17] and different simulations at 298K (except the data for Berger model is from simulation of POPC:POPS (4:1) mixture at 310K [61, 116]). The order parameter values from systems without calcium are set as the zero point of y-axis, except for the α-carbon order parameter of POPS (bottom, right) for which both order parameters are shifted such that the lower order parameter is zero without additional ions. This is to correctly illustrate the forking with different concentrations of calcium. Potassium counterions are used in MacRog simulations and sodium counterions in Lipid14/17 simulations. In CHARMM36 and Berger simulation with added calcium, the charge is neutralized with calcium and monovalent counterions are not present.

ions is observed in all simulation models, despite significant discrepancies in the headgroup structures produced in salt-free simulations [68]. The divergent response of the Berger model may arise from the ring like structures observed in the headgroup region in this model (Fig. 6 in Ref. 35). Therefore, we conclude that improvement of force fields is necessary to correctly capture the interactions between the PS headgroup and calcium ions in MD simulations.

CONCLUSIONS

Here, we used the headgroup C–H bond order parameters and the open collaboration approach to evaluate the quality of the headgroup structure and the ion binding affinity in available PS MD models. The main advantage of this approach is the direct connection between the accurately measurable experimental order parameters and the simulations, which reduces the ambiguity in the interpretation of experiments.

First, we complemented the available experimental information [7, 17] by measuring the signs of the PS headgroup order parameters, and then proceeded to compare MD simulation results from several force fields to the experimental data This revealed that none of the force fields reproduce the PS headgroup order parameters within the experimental accuracy. However, the best models for the serine headgroup suggested a characteristic rigid conformation for its carboxyl group. Comparison to the experimentally observed order parameters in POPC:POPS (5:1) bilayers at varying ion concentrations [17] then showed that the tested MD force fields overestimate the cation binding affinity to these bilayers with two exceptions: 1) the MacRog simulation with potassium coun-

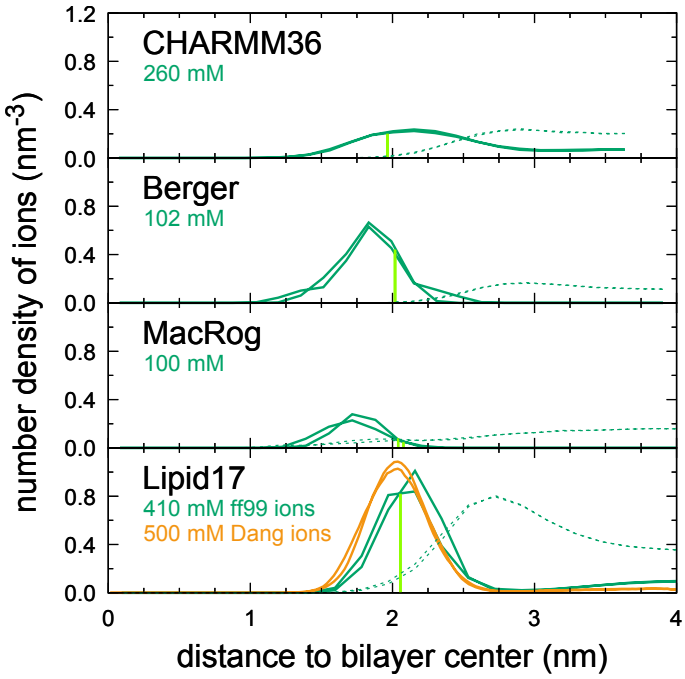

FIG. 10: Number density profiles of Ca^{2+} (solid line) and Cl^{-} (dashed line) from POPC:POPS (5:1) mixtures simulated with different force fields. The vertical green bars indicate the location of the phosphate density peak. The smallest simulated $CaCl_2$ concentrations are shown. The density profiles for all the simulated concentrations are given in SI figure S18.

terions appears to produce the most realistic monovalent ion binding affinity to PS-containing lipid bilayers, and 2) the CHARMM36 force field with the recently introduced NBfix correction for calcium [64] underestimated the calcium binding affinity. The experimentally measured response of the PS headgroup order parameter to the bound calcium, and to the dilution of bilayer with zwitterionic PC lipids, were not qualitatively reproduced in any of the tested force fields, which underlines the need for more accurate the MD force fields to study the biological functioning of PS lipids. This is in contrast to the previous results with PC lipids, where the experimentally measured headgroup order parameter responses to the bound charge were in qualitative agreement even though the headgroup structures themselves were incorrect and the cation binding affinities overestimated [68].

We expect our results to pave the way for the development of better MD force fields for PS lipids. The quality of conformational ensembles produced by the various models can be evaluated based on the headgroup order parameters, which we hope will to guide the development of force fields towards models that correctly reproduce the PS headgroup structures. The cation binding in the force fields can be improved based on the experimental headgroup order parameter data from POPC:POPS (5:1) mixtures under different cation concentrations. This was already demonstrated for POPC using the electronic continuum correction [109], and a similar study for POPS is being progressed separately [118].

MJ acknowledges financial support from the Emil Aaltonen foundation and and CSC-IT center for science for computational resources. OHSO acknowledges financial support from Academy of Finland (315596), Integrated Structural Biology Research Infrastructure of Helsinki Institute of Life Science (Instruct-HiLIFE), and CSC-IT center for science for computational resources. TJP wishes to acknowledge the use of the Iridis computing resources at the University of Southampton

* samuli.ollila@helsinki.fi

[1] M. A. Lemmon, Nat. Rev. Mol. Cell Biol. **9**, 99 (2008).

[2] P. A. Leventis and S. Grinstein, Annual Review of Biophysics **39**, 407 (2010).

[3] L. Li, X. Shi, X. Guo, H. Li, and C. Xu, Trends in Biochemical Sciences **39**, 130 (2014), ISSN 0968-0004.

[4] T. Yeung, G. E. Gilbert, J. Shi, J. Silvius, A. Kapus, and S. Grinstein, Science **319**, 210 (2008).

[5] H. Zhao, E. K. J. Tuominen, and P. K. J. Kinnunen, Biochemistry **43**, 10302 (2004).

[6] G. P. Gorbenko and P. K. Kinnunen, Chemistry and Physics of Lipids **141**, 72 (2006).

[7] J. L. Browning and J. Seelig, Biochemistry **19**, 1262 (1980).

[8] G. Büldt and R. Wohlgemuth, The Journal of Membrane Biology **58**, 81 (1981), ISSN 1432-1424, URL http://dx.doi.org/10.1007/BF01870972.

[9] H. Hauser, E. Finer, and A. Darke, Biochemical and Biophysical Research Communications **76**, 267 (1977), ISSN 0006-291X, URL http://www.sciencedirect.com/science/article/pii/0006291X77907215.

[10] R. J. Kurland, Biochemical and Biophysical Research Communications **88**, 927 (1979), ISSN 0006-291X, URL http://www.sciencedirect.com/science/article/pii/0006291X79914979.

[11] M. Eisenberg, T. Gresalfi, T. Riccio, and S. McLaughlin, Biochemistry **18**, 5213 (1979).

[12] H. Hauser and G. G. Shipley, Biochemistry **22**, 2171 (1983).

[13] R. Dluhy, D. G. Cameron, H. H. Mantsch, and R. Mendelsohn, Biochemistry **22**, 6318 (1983).

[14] H. Hauser and G. Shipley, Biochimica et Biophysica Acta (BBA) - Biomembranes **813**, 343 (1985), ISSN 0005-2736, URL http://www.sciencedirect.com/science/article/pii/0005273685902512.

[15] G. W. Feigenson, Biochemistry **25**, 5819 (1986).

[16] J. Mattai, H. Hauser, R. A. Demel, and G. G. Shipley, Biochemistry **28**, 2322 (1989).

[17] M. Roux and M. Bloom, Biochemistry **29**, 7077 (1990).

[18] M. Roux and M. Bloom, Biophys. J. **60**, 38 (1991).

[19] J. M. Boettcher, R. L. Davis-Harrison, M. C. Clay, A. J. Nieuwkoop, Y. Z. Ohkubo, E. Tajkhorshid, J. H. Morrissey, and C. M. Rienstra, Biochemistry **50**, 2264 (2011).

[20] J. Seelig, Cell Biology International Reports **14**, 353 (1990), ISSN 0309-1651, URL http://www.sciencedirect.com/science/article/pii/030916519091204H.

[21] C. G. Sinn, M. Antonietti, and R. Dimova, Colloids and Surfaces A: Physicochemical and Engineering Aspects **282-283**, 410 (2006), a Collection of Papers in Honor of Professor Ivan B. Ivanov (Laboratory of Chemical Physics and Engineering, University of Sofia) Celebrating his Contributions to Colloid and Surface Science on the Occasion of his 70th Birthday.

[22] R. M. Venable, Y. Luo, K. Gawrisch, B. Roux, and R. W. Pastor, The Journal of Physical Chemistry B **117**, 10183 (2013).

[23] T. Piggot, *CHARMM36 POPS simulations (versions 1 and 2) 298 K 1.0 nm LJ switching* (2017), URL https://doi.org/10.5281/zenodo.1129415.

[24] T. Piggot, *CHARMM36 POPS simulations (versions 1 and 2) 298 K 1.0 nm LJ switching with K ions* (2018), URL https://doi.org/10.5281/zenodo.1182654.

[25] S. Lee, A. Tran, M. Allsopp, J. B. Lim, J. Henin, and J. B. Klauda, J. Phys. Chem. B **118**, 547 (2014).

[26] T. Piggot, *CHARMM36-UA POPS simulations (versions 1 and 2) 298 K 1.0 nm LJ switching* (2017), URL https://doi.org/10.5281/zenodo.1129458.

[27] A. Maciejewski, M. Pasenkiewicz-Gierula, O. Cramariuc, I. Vattulainen, and T. Róg, J. Phys. Chem. B **118**, 4571 (2014).

[28] T. Piggot, *MacRog POPS simulations (versions 1 and 2) 298 K with corrected PO not OP tails* (2018), URL https://doi.org/10.5281/zenodo.1283335.

[29] M. Javanainen, *Simulation of a POPS membrane with potassium counterions* (2018), URL https://doi.org/10.5281/zenodo.1434990.

[30] I. Gould, A. Skjevik, C. Dickson, B. Madej, and R. Walker, *Lipid17: A comprehensive amber force field for the simulation of zwitterionic and anionic lipids* (2018), in preparation.

[31] I. S. Joung and T. E. Cheatham, The Journal of Physical Chemistry B **112**, 9020 (2008).

[32] M. S. Miettinen and B. Kav, *Molecular dynamics simulation trajectory of an anionic lipid bilayer: 100 mol% POPS with Na+ counterions using Joung-Cheatham Ions* (2018), B.K. acknowledges financial support from International Max Planck Research School on Multiscale Bio-Systems., URL https://doi.org/10.5281/zenodo.1148495.

[33] J. Åqvist, J. Phys. Chem. **94**, 8021 (1990).

[34] M. S. Miettinen and B. Kav, *Molecular dynamics simulation trajectory of an anionic lipid bilayer: 100 mol% POPS with Na+ counterions using ff99 ions* (2018), B.K. acknowledges financial support from International Max Planck Research School on Multiscale Bio-Systems, URL https://doi.org/10.5281/zenodo.1134869.

[35] P. Mukhopadhyay, L. Monticelli, and D. P. Tieleman, Biophysical Journal **86**, 1601 (2004).

[36] T. Piggot, *Berger POPS simulations (versions 1 and 2) 298 K 1.0 nm cut-off* (2017), URL https://doi.org/10.5281/zenodo.1129425.

[37] I. Chandrasekhar, M. Kastenholz, R. Lins, C. Oostenbrink, L. Schuler, D. Tieleman, and W. Gunsteren, Eur. Biophys. J. **32**, 67 (2003), ISSN 0175-7571.

[38] A. Kukol, J. Chem. Theory Comput. **5**, 615 (2009).

[39] T. J. Piggot, Á. Piñeiro, and S. Khalid, J. Chem. Theory Comput. **8**, 4593 (2012).

[40] T. Piggot, *GROMOS-CKP POPS simulations (versions 1 and 2) 298 K with Berger/Chiu NH3 charges and PME* (2017), URL https://doi.org/10.5281/zenodo.1129431.

[41] T. Piggot, *GROMOS-CKP POPS simulations (versions 1 and 2) 298 K with GROMOS NH3 charges and PME* (2017), URL https://doi.org/10.5281/zenodo.1129435.

[42] J. P. M. Jämbeck and A. P. Lyubartsev, Phys. Chem. Chem. Phys. **15**, 4677 (2013).

[43] T. Piggot, *Slipids POPS simulations (versions 1 and 2) 298 K 1.0 nm cut-off with LJ-PME* (2017), URL https://doi.org/10.5281/zenodo.1129441.

[44] T. Piggot, *CHARMM36 DOPS simulations (versions 1 and 2) 303 K 1.0 nm LJ switching* (2017), URL https://doi.org/10.5281/zenodo.1129411.

[45] T. Piggot, *CHARMM36-UA DOPS simulations (versions 1 and 2) 303 K 1.0 nm LJ switching* (2017), URL https://doi.org/10.5281/zenodo.1129456.

[46] B. Kav and M. S. Miettinen, *Molecular dynamics simulation trajectory of an anionic lipid bilayer: 100 mol% DOPS with Na+ counterions using Joung-Cheetham Ions* (2018), B.K acknowledges financial support from International Max Planck Research School on Multiscale Bio-Systems, URL https://doi.org/10.5281/zenodo.1134871.

[47] B. Kav and M. S. Miettinen, *Molecular dynamics simula-*

tion trajectory of an anionic lipid bilayer: 100 mol% DOPS with Na+ counterions using ff99 Ions (2018), B.K acknowledges financial support from International Max Planck Research School on Multiscale Bio-Systems, URL https://doi.org/10.5281/zenodo.1135142.

[48] T. Piggot, *Berger DOPS simulations (versions 1 and 2) 303 K 1.0 nm cut-off* (2017), URL https://doi.org/10.5281/zenodo.1129419.

[49] T. Piggot, *GROMOS-CKP DOPS simulations (versions 1 and 2) 303 K with Berger/Chiu NH3 charges and PME* (2017), URL https://doi.org/10.5281/zenodo.1129429.

[50] T. Piggot, *GROMOS-CKP DOPS simulations (versions 1 and 2) 303 K with GROMOS NH3 charges and PME* (2017), URL https://doi.org/10.5281/zenodo.1129447.

[51] T. Piggot, *Slipids DOPS simulations (versions 1 and 2) 303 K 1.0 nm cut-off with LJ-PME* (2017), URL https://doi.org/10.5281/zenodo.1129439.

[52] F. Favela-Rosales, *MD simulation trajectory of a fully hydrated DOPS bilayer: SLIPIDS, Gromacs 5.0.4. 2017.* (2017), URL https://doi.org/10.5281/zenodo.495510.

[53] J. J. López Cascales, J. García de la Torre, S. J. Marrink, and H. J. C. Berendsen, The Journal of Chemical Physics **104**, 2713 (1996).

[54] S. A. Pandit and M. L. Berkowitz, Biophysical Journal **82**, 1818 (2002).

[55] U. R. Pedersen, C. Leidy, P. Westh, and G. H. Peters, Biochimica et Biophysica Acta (BBA) - Biomembranes **1758**, 573 (2006).

[56] P. T. Vernier, M. J. Ziegler, and R. Dimova, Langmuir **25**, 1020 (2009).

[57] A. Martín-Molina, C. Rodríguez-Beas, and J. Faraudo, Biophysical Journal **102**, 2095 (2012).

[58] P. Jurkiewicz, L. Cwiklik, A. Vojtíšková, P. Jungwirth, and M. Hof, Biochimica et Biophysica Acta (BBA) - Biomembranes **1818**, 609 (2012).

[59] J. Pan, X. Cheng, L. Monticelli, F. A. Heberle, N. Kucerka, D. P. Tieleman, and J. Katsaras, Soft Matter **10**, 3716 (2014).

[60] S. Vangaveti and A. Travesset, The Journal of Chemical Physics **141**, 245102 (2014).

[61] A. Melcrová, S. Pokorna, S. Pullanchery, M. Kohagen, P. Jurkiewicz, M. Hof, P. Jungwirth, P. S. Cremer, and L. Cwiklik, Sci. Reports **6**, 38035 (2016).

[62] M. L. Valentine, A. E. Cardenas, R. Elber, and C. R. Baiz, Biophysical Journal **115**, 1541 (2018), ISSN 0006-3495, URL http://www.sciencedirect.com/science/article/pii/S0006349518310221.

[63] M. J. Hallock, A. I. Greenwood, Y. Wang, J. H. Morrissey, E. Tajkhorshid, C. M. Rienstra, and T. V. Pogorelov, Biochemistry **57**, 6897 (2018).

[64] S. Kim, D. Patel, S. Park, J. Slusky, J. Klauda, G. Widmalm, and W. Im, Biophysical Journal **111**, 1750 (2016), ISSN 0006-3495, URL http://www.sciencedirect.com/science/article/pii/S0006349516307615.

[65] J. B. Klauda, R. M. Venable, J. A. Freites, J. W. O'Connor, D. J. Tobias, C. Mondragon-Ramirez, I. Vorobyov, A. D. MacKerell Jr, and R. W. Pastor, J. Phys. Chem. B **114**, 7830 (2010).

[66] O. Berger, O. Edholm, and F. Jähnig, Biophys. J. **72**, 2002 (1997).

[67] A. Botan, F. Favela-Rosales, P. F. J. Fuchs, M. Javanainen, M. Kanduč, W. Kulig, A. Lamberg, C. Loison, A. Lyubartsev, M. S. Miettinen, et al., J. Phys. Chem. B **119**, 15075 (2015).

[68] A. Catte, M. Girych, M. Javanainen, C. Loison, J. Melcr, M. S. Miettinen, L. Monticelli, J. Maatta, V. S. Oganesyan, O. H. S. Ollila, et al., Phys. Chem. Chem. Phys. **18**, 32560 (2016).

[69] O. S. Ollila and G. Pabst, Biochimica et Biophysica Acta (BBA) - Biomembranes **1858**, 2512 (2016).

[70] T. J. Piggot, J. R. Allison, R. B. Sessions, and J. W. Essex, Journal of Chemical Theory and Computation **13**, 5683 (2017).

[71] H. U. Gally, G. Pluschke, P. Overath, and J. Seelig, Biochemistry **20**, 1826 (1981).

[72] P. Scherer and J. Seelig, EMBO J. **6** (1987).

[73] J. J. Madsen, *MD simulations of bilayers containing PC/PS mixtures and CaCl_2: 150POPC_150POPS_neutral* (2019), URL https://doi.org/10.5281/zenodo.2542164.

[74] T. Piggot, *CHARMM36 POPS/POPC simulations (versions 1 and 2) 298 K 1.0 nm LJ switching with K ions* (2018), URL https://doi.org/10.5281/zenodo.1182658.

[75] T. Piggot, *CHARMM36 POPS/POPC simulations (versions 1 and 2) 298 K 1.0 nm LJ switching with Na ions* (2018), URL https://doi.org/10.5281/zenodo.1182665.

[76] J. J. Madsen, *MD simulations of bilayers containing PC/PS mixtures and CaCl_2: 250POPC_50POPS_0.15MCaCl_2* (2019), URL https://doi.org/10.5281/zenodo.2542176.

[77] J. J. Madsen, *MD simulations of bilayers containing PC/PS mixtures and CaCl_2: 250POPC_50POPS_1MCaCl_2* (2019), URL https://doi.org/10.5281/zenodo.2542135.

[78] J. J. Madsen, *MD simulations of bilayers containing PC/PS mixtures and CaCl_2: 250POPC_50POPS_neutral* (2019), URL https://doi.org/10.5281/zenodo.2542151.

[79] M. Javanainen, *Simulation of a POPC bilayer at 298K, lipid model by Maciejewski and Rog* (2018), URL https://doi.org/10.5281/zenodo.1167532.

[80] M. Javanainen, *Simulations of popc/pops membranes with cacl_2.* (2017), URL https://doi.org/10.5281/zenodo.1409551.

[81] C. J. Dickson, B. D. Madej, A. A. Skjevik, R. M. Betz, K. Teigen, I. R. Gould, and R. C. Walker, J. Chem. Theory Comput. **10**, 865 (2014).

[82] B. Kav and M. S. Miettinen, *Amber Lipid17 Simulations of POPC/POPS Membranes with KCl Counterions* (2018), B.K acknowledges financial support from International Max Planck Research School on Multiscale Bio-Systems, URL https://doi.org/10.5281/zenodo.1250969.

[83] B. Kav and M. S. Miettinen, *Amber Lipid17 Simulations of POPC/POPS Membranes with NaCl Counterions* (2018), B.K acknowledges financial support from International Max Planck Research School on Multiscale Bio-Systems, URL https://doi.org/10.5281/zenodo.1250975.

[84] B. Kav and M. S. Miettinen, *Amber Lipid17 Simulations of POPC/POPS Membranes with CaCl2* (2018), B.K acknowledges financial support from International Max Planck Research School on Multiscale Bio-Systems, URL https://doi.org/10.5281/zenodo.1438848.

[85] J. Melcr, *Molecular dynamics simulations of lipid bilayers containing POPC and POPS with the lipid17 force field, only counterions, and CaCl2 concentrations* (2018), URL https://doi.org/10.5281/zenodo.1487761.

[86] D. E. Smith and L. X. Dang, J. Chem. Phys **100**, 3757 (1994), URL http://scitation.aip.org/content/aip/journal/jcp/100/5/10.1063/1.466363.

[87] L. X. Dang, G. K. Schenter, V.-A. Glezakou, and J. L. Fulton,

J. Phys. Chem. B **110**, 23644 (2006), ISSN 1520-6106, URL http://dx.doi.org/10.1021/jp064661f.

[88] D. P. Tieleman, H. J. Berendsen, and M. S. Sansom, Biophys. J. **76**, 1757 (1999).

[89] O. O. H. Samuli, *POPC:POPS (4:1) simulation with Berger model at 310K* (2018), URL https://doi.org/10.5281/zenodo.1475285.

[90] C. Lukasz, *MD simulation trajectory of a POPC/POPS (4:1) bilayer with 102mM CaCl2, Berger force field for lipids, scaled charges for Ca2+ and Cl-* (2017), URL https://doi.org/10.5281/zenodo.887398.

[91] C. Lukasz, *MD simulation trajectory of a POPC/POPS (4:1) bilayer with 715mM CaCl2, Berger force field for lipids, scaled charges for Ca2+ and Cl-* (2017), URL https://doi.org/10.5281/zenodo.887400.

[92] T. Piggot, *GROMOS-CKP POPS/POPC simulations (versions 1 and 2) 298 K with GROMOS NH3 charges and PME* (2018), URL https://doi.org/10.5281/zenodo.1283333.

[93] T. Piggot, *GROMOS-CKP POPS/POPC simulations (versions 1 and 2) 298 K with Berger/Chiu NH3 charges and PME* (2018), URL https://doi.org/10.5281/zenodo.1283331.

[94] S. V. Dvinskikh, H. Zimmermann, A. Maliniak, and D. Sandstrom, J. Magn. Reson. **168**, 194 (2004).

[95] J. D. Gross, D. E. Warschawski, and R. G. Griffin, J. Am. Chem. Soc. **119**, 796 (1997).

[96] T. M. Ferreira, F. Coreta-Gomes, O. H. S. Ollila, M. J. Moreno, W. L. C. Vaz, and D. Topgaard, Phys. Chem. Chem. Phys. **15**, 1976 (2013).

[97] T. M. Ferreira, R. Sood, R. Bärenwald, G. Carlström, D. Topgaard, K. Saalwächter, P. K. J. Kinnunen, and O. H. S. Ollila, Langmuir **32**, 6524 (2016).

[98] M. Bak, J. T. Rasmussen, and N. C. Nielsen, Journal of Magnetic Resonance **147**, 296 (2000), ISSN 1090-7807, URL http://www.sciencedirect.com/science/article/pii/S1090780700921797.

[99] ohsOllila and et al., *Match github repository*, URL https://github.com/NMRLipids/MATCH.

[100] N. Michaud-Agrawal, E. J. Denning, T. B. Woolf, and O. Beckstein, Journal of Computational Chemistry **32**, 2319 (2011), https://onlinelibrary.wiley.com/doi/pdf/10.1002/jcc.21787, URL https://onlinelibrary.wiley.com/doi/abs/10.1002/jcc.21787.

[101] Richard J. Gowers, Max Linke, Jonathan Barnoud, Tyler J. E. Reddy, Manuel N. Melo, Sean L. Seyler, Jan Domański, David L. Dotson, Sébastien Buchoux, Ian M. Kenney, et al., in *Proceedings of the 15th Python in Science Conference*, edited by Sebastian Benthall and Scott Rostrup (2016), pp. 98 – 105.

[102] M. Abraham, D. van der Spoel, E. Lindahl, B. Hess, and the GROMACS development team, *GROMACS user manual version 5.0.7* (2015), URL www.gromacs.org.

[103] H. Akutsu and J. Seelig, Biochemistry **20**, 7366 (1981).

[104] C. Altenbach and J. Seelig, Biochemistry **23**, 3913 (1984).

[105] J. Seelig, P. M. MacDonald, and P. G. Scherer, Biochemistry **26**, 7535 (1987).

[106] F. Borle and J. Seelig, Chemistry and Physics of Lipids **36**, 263 (1985).

[107] P. M. Macdonald and J. Seelig, Biochemistry **26**, 1231 (1987).

[108] M. Roux and J.-M. Neumann, FEBS Letters **199**, 33 (1986).

[109] J. Melcr, H. Martinez-Seara, R. Nencini, J. Kolafa, P. Jungwirth, and O. H. S. Ollila, The Journal of Physical Chemistry B **122**, 4546 (2018).

[110] P. G. Scherer and J. Seelig, Biochemistry **28**, 7720 (1989).

[111] M. Roux, J.-M. Neumann, M. Bloom, and P. F. Devaux, European Biophysics Journal **16**, 267 (1988).

[112] M. Loosley-Millman, R. Rand, and V. Parsegian, Biophysical Journal **40**, 221 (1982).

[113] R. Rand and V. Parsegian, Biochimica et Biophysica Acta (BBA) - Reviews on Biomembranes **988**, 351 (1989).

[114] J. Melcr, *POPC lipid membrane, 303K, Charmm36 force field, simulation files and 200 ns trajectory for Gromacs MD simulation engine v5.1.2* (2016), URL https://doi.org/10.5281/zenodo.153944.

[115] H. I. Petrache, S. Tristram-Nagle, K. Gawrisch, D. Harries, V. A. Parsegian, and J. F. Nagle, Biophysical Journal **86**, 1574 (2004).

[116] S. Ollila, M. T. Hyvönen, and I. Vattulainen, J. Phys. Chem. B **111**, 3139 (2007).

[117] G. Cevc, Biochim. Biophys. Acta - Rev. Biomemb. **1031**, 311 (1990).

[118] Melcr and et al., *Ecc-lipids github repository*, URL https://github.com/jmelcr/ecc_lipids.

ToDo

P.

1. Replacing the "literature" with "from Ref X" has been suggested https://github.com/NMRLipids/NMRlipidsIVotherHGs/issues/34. We can do this just before submission when citation numbers will not change anymore. 5

2. After we know which force field is used for POPC in GROMOS-CKP simulations, we might be able to add GROMOS-CKP data into this plot. 8